DOI: 10.15669/pnst.7.286

Progress in Nuclear Science and Technology
Volume 7 (2025) pp. 286-292

ARTICLE

Power-density enhancement of composite materials using open-cell foams for thermochemical energy storage

Kyosuke Mochizuki [a], Shigehiko Funayama [b *], Massimiliano Zamengo [c], Hiroki Takasu [b] and Yukitaka Kato [b]

[a] Graduate Major in Nuclear Engineering, Department of Chemical Science and Engineering, Institute of Science Tokyo, N1-22 2-12-1, Ookayama, Meguro-ku, Tokyo 152-8550, Japan; [b] Laboratory for Zero-Carbon Energy, Institute of Integrated Research, Institute of Science Tokyo, N1-22 2-12-1, Ookayama, Meguro-ku, Tokyo 152-8550, Japan; [c] School of Materials and Chemical Technology, Institute of Science Tokyo, S8-29 2-12-1, Ookayama, Meguro-ku, Tokyo 152-8550, Japan

Thermal energy storage technologies are essential for the efficient use of surplus heat and renewable energy. Thermochemical energy storage using a calcium hydroxide/water/calcium oxide ($Ca(OH)_2/H_2O/CaO$) reaction system possesses high energy storage density and is suitable for long-term storage. However, pure $Ca(OH)_2$ powder has a low thermal conductivity and poor bulk stability with volume changes and agglomeration. In this study, we focused on composite materials using $Ca(OH)_2$ and silicon–impregnated silicon carbide (Si–SiC) foams to address aforementioned shortcomings. This study investigated the effects of foam porosity (89–95%) on the heat storage/output rate of the composite and cycle durability using a laboratory-scale packed bed reactor. The composites with Si–SiC foam porosities of 92 and 95% exhibited the highest heat storage rate during $Ca(OH)_2$ dehydration of 0.60 kW L_{bed}^{-1}, which is 1.4 times that of pure $Ca(OH)_2$ powder. The composite with a Si–SiC foam porosity of 95% also exhibited the highest heat output rate during CaO hydration of 1.15 kW L_{bed}^{-1}, which is 1.5 times that of the pure powder. The composite foam maintained a high reactivity and did not form centimeter-scale agglomerates during the 15 cycles. The results of this study provide significant insights into the optimization of foam structures in composites with high power density and cycle durability for thermochemical energy storage.

Keywords: thermochemical energy storage; calcium hydroxide; silicon carbide foam; foam porosity; packed bed reactor

1. Introduction

The use of renewable energy is currently being promoted worldwide to achieve the decarbonization of society. However, energy generation from renewable energy sources is mismatched with demand. Thus, surplus energy must be stored for reuse on demand. Thermal energy storage technologies are required for the efficient use of surplus heat and renewable energy. Thermochemical energy storage (TCES) has attracted considerable research interest. TCES uses reversible gas–solid reactions to store thermal energy [1,2]. Here, we focused on TCES with a calcium hydroxide/water/calcium oxide ($Ca(OH)_2/H_2O/CaO$) reaction system [3]. This system uses endothermic dehydration for heat storage and exothermic hydration for heat output (Eq. 1):

$$Ca(OH)_2(s) \rightleftharpoons CaO(s) + H_2O(g);\ \Delta H_r = 104\ \text{kJ mol}^{-1} \quad (1)$$

This system possesses a high energy-storage density (1 MJ L^{-1} [4]) and long-term storage capability. However, pure $Ca(OH)_2$ powder exhibits low thermal conductivity [5,6], cohesive properties that cause agglomeration [7], and bulk instability during repetitive reactions [8,9]. In the literature, composite materials using vermiculite [10], silicon carbide honeycombs [11], tetraethoxysilane/silane coupling agent [12], sodium silicate [13], SiO_2 nanoparticles [7], kaolinite [14], and encapsulated granules [15] have been studied.

In previous studies, we focused on composites using $Ca(OH)_2$ and silicon–impregnated silicon carbide (Si–SiC) foams [4,16]. The composites were observed to exhibit superior heat storage/output rates and cycle stability compared to pure $Ca(OH)_2$ powder. However, to the best of our knowledge, the effects of the porosity of the Si–SiC foam on the power density of the composite have not been investigated. This experimental study aimed to investigate the effects of foam porosity ranging between 89–95% on the volumetric heat storage/output rate of the composite using a laboratory-scale packed bed reactor. Additionally, the cycle durability of the composite with the highest power density over 15 cycles is evaluated.

*Corresponding author. E-mail: funayama.s.aa@m.titech.ac.jp

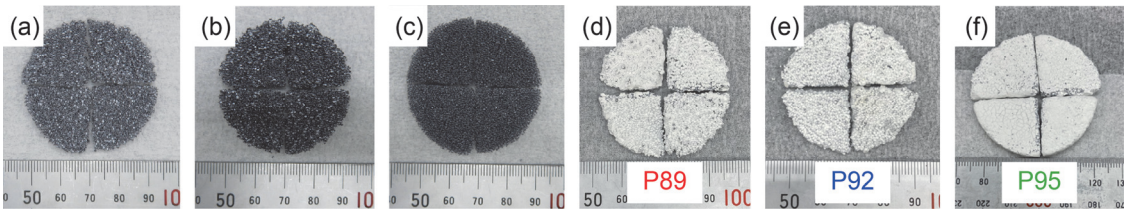

Figure 1. Foam supports and composite materials: Si–SiC foams with porosities of (a) 89%, (b) 92%, and (c) 95%; composites with $Ca(OH)_2$ and Si–SiC foams: (d) P89, (e) P92, and (f) P95.

2. Materials and methods

2.1. Materials

A calcium hydroxide slurry (Shiraishi Central Laboratory Co., Ltd.) was used to prepare the composite materials and is referenced as $Ca(OH)_2$ powder. A dispersing agent was employed to adjust the viscosity of the slurry to approximately 1000 mPa s. The reference $Ca(OH)_2$ powder was prepared by drying the slurry and sieving it to 53–150 μm, denoted as CP. Disk-shaped Si–SiC foams, which were divided into four parts, were manufactured by NGK Insulators, Ltd. Three different foams with porosities of 89, 92, and 95% were prepared (**Figures 1 (a)–(c)**). The pore diameters of the foams were 0.4 mm. The diameter and thickness of the disk-shaped samples were 44 and 6 mm, respectively. Three cylindrical samples comprising eight-disk foams were used in the experiments with a packed bed reactor. The Si–SiC foams were impregnated with a $Ca(OH)_2$ slurry and dried at 120 °C for at least 12 h. The composites prepared in this study are shown in **Figures 1 (d)–(f)**. The composites employing the Si–SiC foams with porosities of 89, 92, and 95% are denoted as P89, P92, and P95, respectively. The main properties of the samples are presented in **Table 1**.

Table 1. Main properties of the materials.

	CP	P89	P92	P95
Mass of $Ca(OH)_2$ [g]	51.2	41.5	48.2	53.9
Mass of composite [g]	-	59.1	66.2	64.2
Bed height [mm]	48	47	49	48
Volume [cm^3]	96	73	75	82

2.2. Experimental apparatus

The experimental apparatus employed in this study is shown in **Figure 2**. A packed bed reactor was used to measure the heat storage, heat output rate, and cycle durability of the developed materials at the laboratory scale. The reactor had an inner diameter and height of 48 and 70 mm, respectively. Eight composite disks were loaded into the reactor. Thermocouples (type K, ø1.0 mm, ±0.75%, OMEGA Engineering, Inc.) were installed in the reactor to monitor the bed temperature. The temperature of the central side (T_4) was controlled using a thermostat and heater placed around the outer wall of the reactor. Prior to the experiments, a vacuum pump was employed to remove the air inside the system. Because only water vapor was present in the system, the pressure inside was determined from the saturated water vapor pressure corresponding to the water temperature in the reservoir. The mass change of the reactor during the reactions was measured using an electronic balance (±0.1 g, MS16001 L/02, Mettler Toledo). The pressure inside the system was measured using two pressure sensors (±0.2 kPa, PA-750-302R, Nidec Copal Electronics). To prevent the condensation of water vapor, the pipes between the reactor chamber and reservoir were maintained at >120 °C using ribbon heaters and insulators. The water temperature of the reservoir was maintained at a constant value using chillers and heaters during dehydration and hydration, respectively.

2.3. Experimental conditions

The reactor was preheated to 480 °C at a water vapor pressure of >90 kPa before dehydration. The dehydration reaction was initiated by depressurizing the reactor connected to a water reservoir at a temperature of 20 °C (T_w). The water vapor produced in the reactor during dehydration was transferred to the water reservoir and

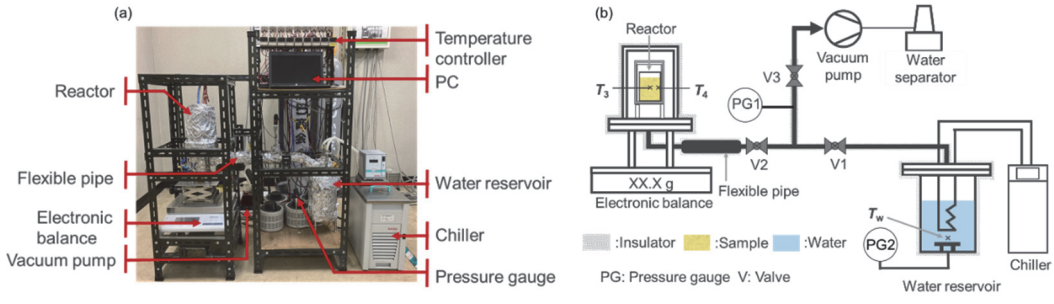

Figure 2. Experimental apparatus: (a) photograph and (b) schematic diagram.

condensed.

Prior to hydration, the reactor was preheated to 350 °C. The hydration reaction was initiated by opening a valve (V1) and introducing water vapor at a pressure of 58 kPa into the reactor. The experimental conditions of 15 cycles was similar to that of our previous study [16].

2.4. Performance evaluation method

The reaction conversion change during dehydration, Δx_{d} [−], and hydration, Δx_{h} [−], was calculated using Eq. 2:

$$\Delta x_{(\mathrm{d,h})} = \frac{\Delta m / M_{\mathrm{H_2O}}}{m_{\mathrm{Ca(OH)_2}} / M_{\mathrm{Ca(OH)_2}}}, \tag{2}$$

where Δm [g], $m_{\mathrm{Ca(OH)_2}}$ [g], $M_{\mathrm{H_2O}}$ [g mol^{-1}], and $M_{\mathrm{Ca(OH)_2}}$[g mol^{-1}] denote the mass change of the reaction chamber, initial mass of the $Ca(OH)_2$ sample, molar mass of water, and molar mass of $Ca(OH)_2$, respectively.

The estimated heat storage density, Q [kJ L_{bed}^{-1}], was calculated using Eq. (3) with the reaction enthalpy, ΔH_{r} [kJ mol^{-1}], and bed volume, V_{bed} [m^3]:

$$Q = \Delta H_{\mathrm{r}} \frac{m_{\mathrm{Ca(OH)_2,ini}}}{M_{\mathrm{Ca(OH)_2}}} \frac{1}{V_{\mathrm{bed}}}. \tag{3}$$

The heat storage density, q_{d} [kJ L_{bed}^{-1}], and heat output density, q_{h} [kJ L_{bed}^{-1}], are defined as follows:

$$q_{(\mathrm{d,h})} = Q \cdot \Delta x_{(\mathrm{d,h})}. \tag{4}$$

The heat storage rate, w_{d} [kW L_{bed}^{-1}], and heat output rate, w_{h} [kW L_{bed}^{-1}], are defined using the $q_{(\mathrm{d,h})}$ and reaction time, $t_{(\mathrm{d,h})}$ [s], as described below:

$$w_{(\mathrm{d,h})} = q_{(\mathrm{d,h})} / t_{(\mathrm{d,h})}. \tag{5}$$

3. Results and discussion

3.1. Heat storage and output performance

The reaction conversion changes and center temperatures (T_3) of CP, P89, P92, and P95 during dehydration and hydration are shown in **Figure 3**. After the start of dehydration, T_3 considerably decreased from the initial temperature and later gradually increased until it reached the initial temperature. All the materials exhibited a high final conversion change of >80%. The minimum T_3 values for CP, P89, P92, and P95 were 384, 392, 396, and 391 °C, respectively, indicating that the minimum T_3 of the composites was higher than that of CP. The time required until T_3 and the conversion change reached a steady state differed significantly for CP and the composites, which may be because Si–SiC improved the heat transfer of the bed.

After the start of hydration, T_3 increased instantaneously and approached the chemical equilibrium temperature corresponding to the water vapor pressure. The obtained T_3 of CP, P89, P92, and P95 were 480, 480, 475, and 479 °C, respectively. T_3 plateaued during hydration and later decreased to the initial temperature after the completion of the reaction. All the samples exhibited high final conversion changes of >80%. The times required to complete the reactions were approximately 100, 40, 45, and 50 min for CP, P89, P92, and P95, respectively, thereby suggesting that the heat transfer was improved by the Si–SiC foams.

Figure 4 shows the volumetric heat storage density, q_{d}, and heat output density, q_{h}, of the materials. The q_{d} and q_{h} of the composites increased more rapidly than that of CP. The estimated heat storage density, Q, of CP, P89, P92, and P95 was 832, 798, 903, and 913 kJ L_{bed}^{-1}, respectively, indicating that the composites had a higher power density performance than CP without compromising the estimated heat storage density.

The w_{d} and w_{h} at 5 min of the materials with different porosities of Si–SiC foam averaged over the first 10 cycles are shown in **Figure 5**, where the values of CP are plotted at a foam porosity of 100%. The w_{d} at 5 min of CP, P89, P92, and P95 were 0.42, 0.52, 0.60, and 0.60 kW L_{bed}^{-1}, respectively. The maximum w_{d} was observed when the foam porosity was 92% and 95%, and the maximum value was 1.4 times that of CP. The w_{h} at 5 min of CP, P89, P92, and P95 was 0.78, 0.90, 0.90, and 1.15 kW L_{bed}^{-1}, respectively. The maximum w_{h} was observed when the foam porosity was 95%, and the maximum value was 1.5 times that of CP.

These results reveal that the Si–SiC foams improved

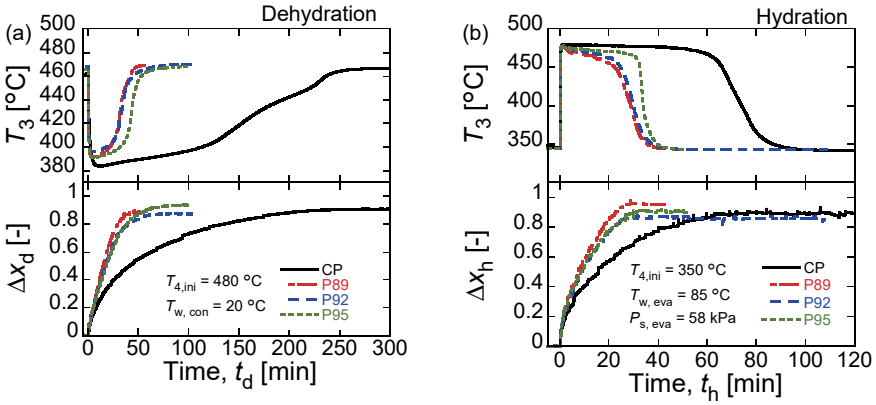

Figure 3. Center temperature and conversion change: (a) dehydration and (b) hydration.

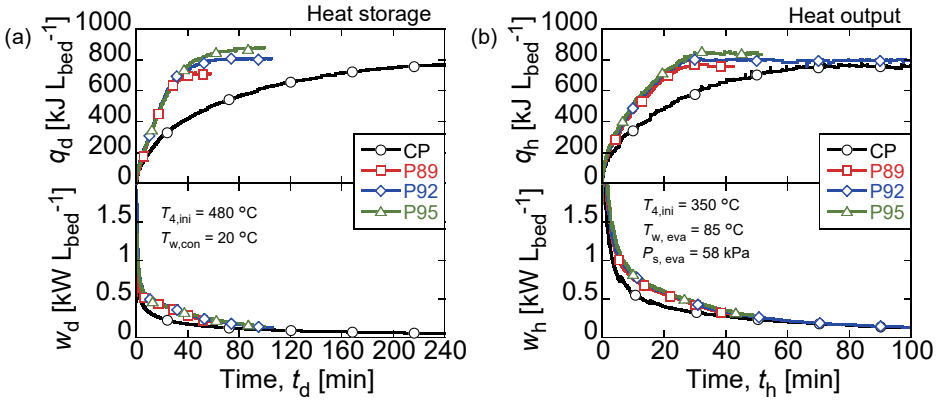

Figure 4. Heat storage and heat output performance: (a) heat storage and (b) heat output.

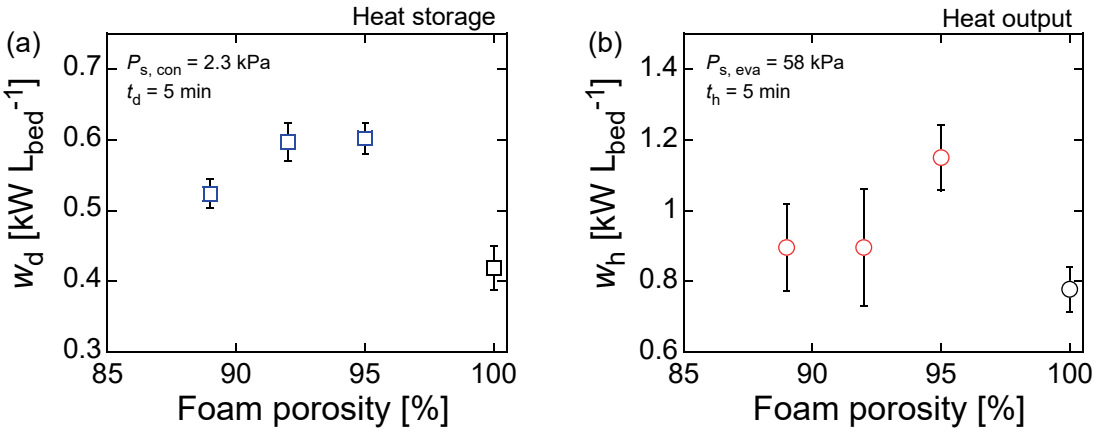

Figure 5. Heat storage and output rates of the materials with different foam porosities averaged over the first 10 cycles: (a) heat storage and (b) heat output. The CP values are plotted at a foam porosity of 100%.

the w_d and w_h of the composites compared to CP. The addition of 5 vol% Si–SiC significantly increased both w_d and w_h. However, w_d and w_h did not improve significantly with the addition of Si–SiC between 5–11 vol%, even though the effective thermal conductivity improved as the volume fraction of Si–SiC increased. This could be explained by the fact that w_d and w_h are proportional to the estimated heat storage density, Q, which decreases with increasing volume fraction of Si–SiC, as expressed in Eq. (5). These results suggest that a decrease in Q has a greater impact on w_d and w_h than an increase in the effective thermal conductivity at Si–SiC fractions of 5–11 vol%. Furthermore, the results reveal that there could no longer be a trade-off between Q and w for a porosity of <95% under the test conditions of this study.

3.2. Cycle durability

P95 exhibited the highest heat storage/output rate. In this section, the cycle durability of P95 is compared to that of CP. **Figure 6** shows the final conversion change over 15 cycles. P95 retained a high reactivity of >86% after the second cycle, as CP did. The final conversion change of CP and P95 for the first cycle was severely low, which could be attributed to the mass transfer of water vapor through $CaO/Ca(OH)_2$ materials being limited. The samples did not reach full conversion changes, mainly because of the carbonation of $CaO/Ca(OH)_2$ and losses in the loading processes of the samples into the reactor.

The X-ray diffraction (XRD) pattern of P95 after 15 cycles is shown in **Figure 7**. The sample peaks of P95 after the cycles correlated with those of the uncycled $Ca(OH)_2$ powder and Si–SiC foam, except for calcium carbonate. The results show that the Si–SiC foams were chemically inert and suitable for TCES with $CaO/Ca(OH)_2$ under the conditions used in this study.

The CP and P95 loaded into the reactor before and after the 15 cycles are shown in **Figure 8**. The CP formed agglomerates of several centimeters over 15 cycles, whereas no centimeter-scale agglomerates were observed in the P95 bed. The volume changes in CP and P95 were 8 and 6%, respectively. These results reveal that the Si–SiC foam decreased the volume change and formation of centimeter-scale agglomerates, thereby resulting in an increased stability of the composite bed.

The agglomeration effects inside the foam pores of P95 were evaluated using the specific surface area and scanning electron microscopy (SEM) observations of the $Ca(OH)_2$

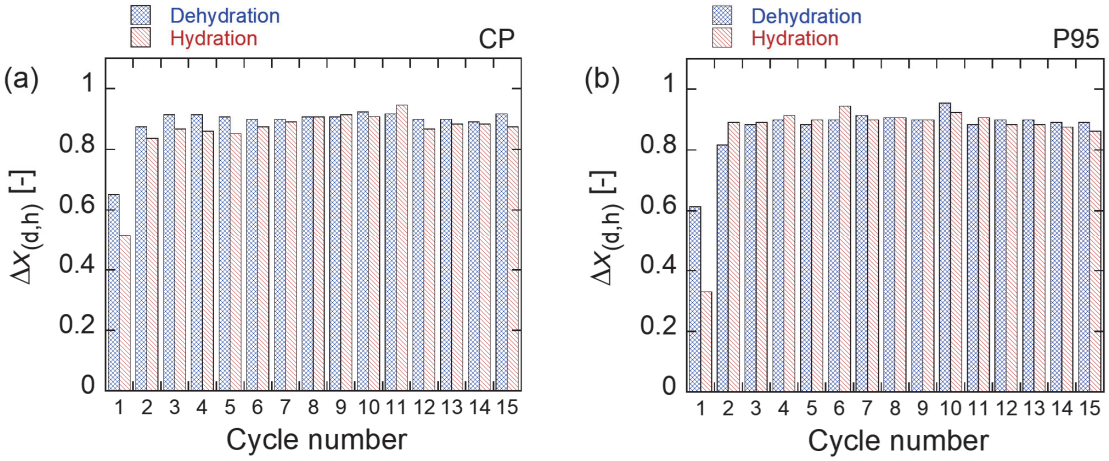

Figure 6. Final conversion change over 15 cycles: (a) CP and (b) P95.

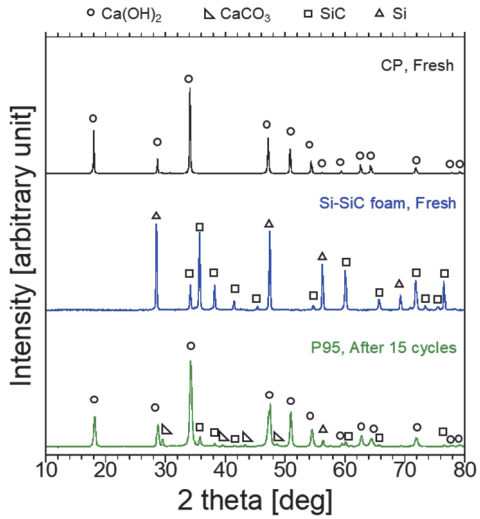

Figure 7. XRD patterns of P95 after 15 cycles.

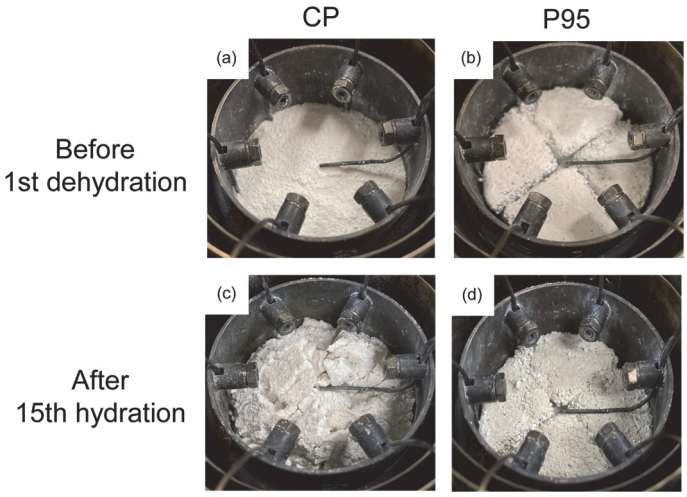

Figure 8. Bulk appearance: (a) CP before 1st dehydration; (b) P95 before 1st dehydration; (c) CP after 15th hydration; and (d) P95 after 15th hydration.

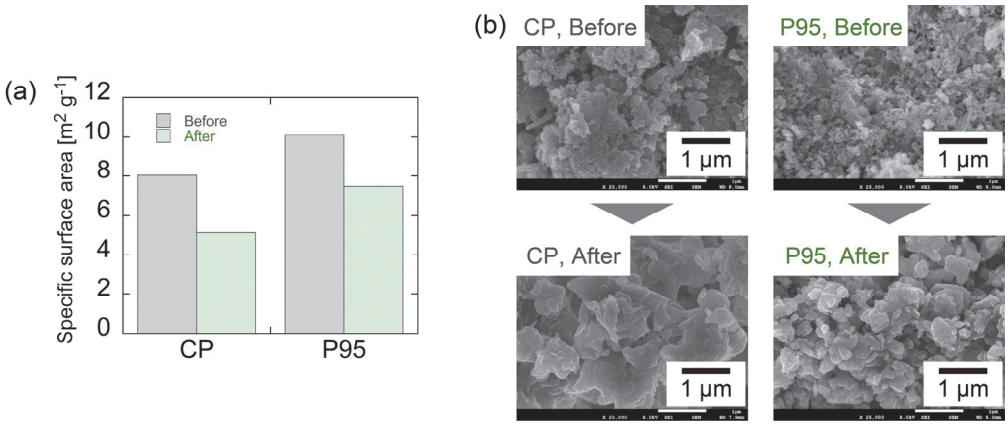

Figure 9. Agglomeration effects of CP and $Ca(OH)_2$ in the foam pores of P95: (a) specific surface area and (b) SEM micrographs.

samples in P95. The specific surface areas of the $Ca(OH)_2$ samples removed from the center of the bed of the CP and P95 samples before and after 15 cycles are shown in **Figure 9 (a)**. The specific surface areas of the CP and P95 samples decreased after 15 cycles. **Figure 9 (b)** shows the SEM micrographs of the $Ca(OH)_2$ samples before and after 15 cycles. The particle size of $Ca(OH)_2$ in P95 increased after the cycles, as CP did. These results suggest

the agglomeration of the $Ca(OH)_2$ sample inside the foam pores of P95. However, the agglomeration of $Ca(OH)_2$ inside the foam pores of P95 did not significantly influence the conversion change, as previously described.

Future studies should increase the diversity of the foam porosity to determine the optimal porosity that can maximize the heat storage/output rates. Further studies will focus on optimizing the foam geometry, such as the pore size and pore density, and on improving the preparation procedure of the composite to improve the estimated heat storage density. Additionally, the durability of longer cycles and reduction of agglomeration inside the foam pores will be addressed in future works.

4. Conclusions

In this study, we developed composite materials using $Ca(OH)_2$ and thermally conductive Si–SiC foams for thermochemical energy storage. The primary objective was to investigate the effects of the foam porosity on the heat storage and output rates of the composite. Si–SiC foams with foam porosities of 89%, 92%, and 95% were employed, and the resulting composites, P89, P92, and P95, were synthesized, respectively.

The heat storage rate (after 5 min during dehydration) of P89, P92, and P95 was 0.52, 0.60, and 0.60 kW L_{bed}^{-1}, which was 1.2, 1.4, and 1.4 times that of a referenced pure $Ca(OH)_2$ powder, respectively. The heat output rate (after 5 min during hydration at a pressure of 58 kPa) of P89, P92, and P95 was 0.90, 0.90, and 1.15 kW L_{bed}^{-1}, which was 1.2, 1.2, and 1.5 times that of the pure $Ca(OH)_2$ powder, respectively. Thus, P95 had the highest power density performance for the heat storage/output conditions of the packed bed reactor used in this study, thereby suggesting that a small amount of Si–SiC effectively enhanced the rates without any considerable loss of heat storage density of the composite.

Composite P95 also maintained a high reactivity of >80% after the 2nd cycle, and the XRD patterns did not show any evidence of side reactions, except for calcium carbonate. P95 exhibits a volume change of 6% after 15 cycles. It is suggested that the agglomeration of $CaO/Ca(OH)_2$ inside the foam pores of P95 could occur owing to the reduced specific surface area and increased particle size of $Ca(OH)_2$. However, agglomeration inside the foam did not impact the final conversion change considerably. Furthermore, P95 did not form centimeter-scale agglomerates, unlike the pure $Ca(OH)_2$ powder. These results reveal the high cycle durability of the P95 composite. Our results show that composites with Si–SiC foams can simultaneously increase heat transfer and decrease volume change and centimeter-scale agglomerates.

Acknowledgments

This work was supported by JST-Mirai Program Grant Number JPMJMI21E4, Japan. The authors would like to acknowledge NGK Insulators, Ltd., for providing the foam materials. The authors would also like to acknowledge Shiraishi Central Laboratory Ltd. for preparing the calcium hydroxide slurry.

References

[1] L. André, S. Abanades and G. Flamant, Screening of thermochemical systems based on solid-gas reversible reactions for high temperature solar thermal energy storage, *Renew. Sustain. Energy Rev*. 64 (2016), pp. 703-715.

[2] G. Ervin, Solar heat storage using chemical reactions, *J. Solid State Chem*. 22 (1977), pp. 51-61.

[3] K. Wang, T. Yan, R.K. Li and W.G. Pan, A review for $Ca(OH)_2/CaO$ thermochemical energy storage systems, *J. Energy Storage* 50 (2022), 104612.

[4] S. Funayama, H. Takasu, M. Zamengo, J. Kariya, S.T. Kim and Y. Kato, Composite material for high-temperature thermochemical energy storage using calcium hydroxide and ceramic foam, *Energy Storage* 1 (2019), e53.

[5] H. Ogura, M. Miyazaki, H. Matsuda, M. Hasatani, M. Yanadori and M. Hiramatsu, Experimental study on heat transfer enhancement of the solid reactant particle bed in a chemical heat pump using $Ca(OH)_2/CaO$ reaction, *Kagaku Kogaku Ronbunshu* 17 (1991), pp. 916-923.

[6] F. Schaube, A. Wörner and R. Tamme, High temperature thermochemical heat storage for concentrated solar power using gas–solid reactions, *J. Sol. Energy Eng*. 133 (2011), 031006.

[7] C. Roßkopf, M. Haas, A. Faik, M. Linder and A. Wörner, Improving powder bed properties for thermochemical storage by adding nanoparticles, *Energy Convers. Manag*. 86 (2014), pp. 93-98.

[8] L. Dai, X.F. Long, B. Lou and J. Wu, Thermal cycling stability of thermochemical energy storage system $Ca(OH)_2/CaO$, *Appl. Therm. Eng*. 133 (2018), pp. 261-268.

[9] M. Schmidt and M. Linder, Power generation based on the $Ca(OH)_2/CaO$ thermochemical storage system – Experimental investigation of discharge operation modes in lab scale and corresponding conceptual process design, *Appl. Energy* 203 (2017), pp. 594-607.

[10] J. Kariya, J. Ryu and Y. Kato, Development of thermal storage material using vermiculite and calcium hydroxide, *Appl. Therm. Eng*. 94 (2016), pp. 186-192.

[11] S. Funayama, H. Takasu, S.T. Kim and Y. Kato, Thermochemical storage performance of a packed bed of calcium hydroxide composite with a silicon-based ceramic honeycomb support, *Energy* 201 (2020), 117673.

[12] R. Guo, S. Funayama, S.T. Kim, T. Harada, H. Takasu and Y. Kato, Hydration reactivity enhancement of calcium oxide-based media for thermochemical energy storage, *Energy Storage 3 (2021)*, e232.

[13] Y.A. Criado, M. Alonso and J.C. Abanades, Composite material for thermochemical energy storage using $CaO/Ca(OH)_2$, *Ind. Eng. Chem. Res*. 54 (2015), pp. 9314-9327.

[14] K.G. Sakellariou, Y.A. Criado, N.I. Tsongidis, G. Karagiannakis and A.G. Konstandopoulos, Multi-cyclic evaluation of composite CaO-based structured bodies for thermochemical heat storage via the

$CaO/Ca(OH)_2$ reaction scheme, *Sol. Energy* 146 (2017), pp. 65-78.

[15] S. Afflerbach, K. Afflerbach, R. Trettin and W. Krumm, Improvement of a semipermeable shell for encapsulation of calcium hydroxide for thermochemical heat storage solutions: Material design and evaluation in laboratory and reactor scale, *Sol. Energy* 217 (2021), pp. 208-222.

[16] S. Funayama, M. Schmidt, K. Mochizuki, M. Linder, H. Takasu and Y. Kato, Calcium hydroxide and porous silicon-impregnated silicon carbide-based composites for thermochemical energy storage, *Appl. Therm. Eng*. 220 (2023), 119675.